Geomechanics and Engineering, *Vol. 40, No. 5 (2025) 353-368*
https://doi.org/10.12989/gae.2025.40.5.353

Finite element analysis of longitudinal impact waves in conical rods

Ragab M. Etiwa and Hesham A. Elkaranshawy*

Department of Engineering Mathematics and Physics, Engineering Mechanics Division, Alexandria University, Alexandria, Egypt

(*Received January 14, 2023, Revised February 13, 2025, Accepted February 17, 2025*)

Abstract. In this paper, a finite element formulation for the impact-induced waves in a variable cross-section rod that collides with a rigid mass is provided. The rod has either fixed, free, or deformable support conditions. The analysis is based on St. Venant's contact theory. The effects of boundary conditions, mass ratios, and geometrical shape of the rod upon stress wave propagation, contact force, displacement, and velocity are thoroughly analyzed by illustrative examples. The proposed finite element formulation considers the rod and the struck mass as one system during the contact period to eliminate the discontinuity at the arrival of the impact wave to the contact end, which gives accurate results. Excellent agreement is found between the finite element results and analytical solution using the mode superposition method for the fixed support boundary condition. The results show that the presented formulation can be used to model many systems with variable cross-section rods that are subjected to longitudinal impact. For instance, it can be used as a basis for modeling nanostructures under impact loads, as benchmark templates for crack detection, and for validating approximate analytical solutions.

Keywords: conical rod; finite element analysis; longitudinal impact; stress wave propagation; superposition method

1. Introduction

Machines produce impact loads in their functional operation and can generate forces many times greater than other machines of the same size. These machines have applications in many engineering activities in the structural, mechanical, automotive, and aerospace industries. However, these impact loads could produce degradation effects and premature failure. Rods are widespread elements in these machines, or even the main part of the machine could be a rod-like body, especially in power pulse systems. Such machines are confronted in forging, rock destruction, pile driving, percussive drilling, punching, hydraulic hammering, and drilling devices in the aerospace application to explore the subsurface of the Lunar and Martian (Bruno and Randolph 1999, Krehl 2008, Chiang and Elías 2000, Vila and Malla 2014, Malla and Vila 2017, Liu *et al.* 2022).

The split Hopkinson pressure bar, also known as the Kolsky bar, is the most well-known device that employs longitudinal impact to generate stress waves. It has been widely used for various applications, including determining the dynamic strength of materials at high strain rates, conducting soil testing in geotechnical engineering, and calibrating shock accelerometers (Elkaranshawy and Bajaba 2012, Hu and Eberhard 2004, Ramirez and Rubio-Gonzalez 2006). Additionally, there is an increasing interest in using impact waves in the determination of the mechanical properties of materials, non-destructive testing methods, and crack detection (Akbas 2014, Bajaba and Elkaranshawy 2008, Elkaranshawy 2019, Kumar *et al.* 2017). Notably, the increasing applications of nanorods and functionally graded structures draw attention to modeling them under impact loading (Akbas 2020, Asiri *et al.* 2020).

The wave theory is used by St. Venant to analyze the longitudinal wave propagation in a uniform rod, which is generated by a striking rigid mass at one end of the rod. The assumptions of the analysis include one-dimensional wave propagation and a perfectly plane contact surface. At the instant of impact, the velocity of the struck end of the rod becomes the same as that of the striking block. After that, the struck end and the striking block undergo the same motion during the contact period. Details of this analysis can be accessed in classical books like (Love 1944, Goldsmith 1960, Timoshenko 1937, Graff 1975, Johnson 1972).

St. Venant's contact theory has been utilized to model the longitudinal impact of rods since it most fully reflects the real dynamic processes in colliding bodies (Stepanov *et al.* 2018). Standard analytical methods have been applied to solve St. Venant's model for uniform rods, like D'Alembert's method (elementary wave theory) (Goldsmith 1960, Timoshenko 1937, Graff 1975, Johnson 1972), Laplace transform method (Yang 2008, Schwarz *et al.* 2010, Wang *et al.* 2023), and the separation of variables method (Vila and Malla 2014, Malla and Vila 2017, Timoshenko 1937, Graff 1975). Analytical methods that contain approximations or numerical procedures have been developed, like symbolic computer algebra (Hu *et al.* 1999), the time delay method (Bin Hu and Eberhard 2004), and the modal superposition method (Dechao and Yufeng 1996, Yufeng and Dechao 1998, Korzyuk and Rudzko 2024, Wang, *et al.* 2024). Also, numerical methods have been used to investigate the longitudinal impact, for example, the

*Corresponding author, Professor
E-mail: hesham_elk@alexu.edu.eg

ISSN: 2005-307X (Print), 2092-6219 (Online)

finite difference method (Wang and Tian 2007), the finite element method (Bajaba and Elkaranshawy 2008, Elkaranshawy 2019, Kumar *et al.* 2017, Ramírez and Rubio-Gonzalez 2006, Elkaranshawy and Bajaba 2008, Idesman *et al.* 2010, Elkaranshawy and Bajaba 2012, Ragab and Fayed 2018, Etiwa *et al.* 2021, Etiwa and Elkaranshawy 2022, Etiwa *et al.* 2023), the boundary element method (Gunawan and Hirose 2005), and the dynamic substructure method (Shen and Yin 2014).

Rods composed of combined segments of different materials and/or different cross-sectional areas are frequently encountered in many engineering applications. Modelling wave propagation in these rods attracted some researchers (Goldsmith 1960, Graff 1975, Johnson 1972, Shen and Yin 2014, Sankin and Yuganova 2001, Shen and Yin 2016). In addition, rods of variable cross-sections have various applications. Examples can come in rotor blades, impact tools in power impulse systems, racks and piles of various configurations, and percussion mechanisms. Multisided steel poles used as light posts, power transmission towers, wind towers, and antenna stands have conical box shaped. Furthermore, power pulse systems highly need accurate and effective control of impact loads to increase the efficiency of energy transfer to the process area, which increases the productivity of the machine. Hence, the shape of the shock pulse is adjusted by the geometrical shape of the variable cross-section rod used in pulse generation (Stepanov *et al.* 2018). The propagation characteristics of longitudinal impact waves in variable rods are much more complicated than those in uniform rods.

To understand the longitudinal impact of variable cross-section rods, it is important to consider the longitudinal vibration of variable cross-section rods under various loading conditions. Considering various combinations of end conditions are required in these models, like clamped, free, attached with mass, attached with linear spring, and attached with linear spring and mass. Many analytical methods have been used in the analysis like the elementary wave theory (Guo and Yang 2012, Gan *et al.* 2014, 2016), Love wave theory (Gan *et al.* 2014, 2016, Banerjee *et al.* 2020), Mindlin-Herrmann wave theory (Gan *et al.* 2016, Banerjee *et al.* 2020), Lie symmetry method (Nunes *et al.* 2022), a method based on the Riccati equation (Pala and Kahya 2022). Approximate analytical and numerical methods have also been used, like the Fourier series (Xu *et al.* 2019), series solution (Utyashev 2019, Guo and Yang 2015, Hull 2018), the nonlinear algebraic system, which is solved by numerical procedures (Abdeddine *et al.* 2020), and finite element method (Gan *et al.* 2016, Hull 2018).

Despite the numerous applications of the longitudinal impact of variable cross-section rods, only a few investigations were performed for its solution and analysis. The propagation characteristics of waves in such rods are much more complicated than those in uniform rods. One reason for this fact is that the wave equations governing variable cross-section rods are partial differential equations with variable coefficients, which are difficult to solve analytically (Hu *et al.* 2001). D'Alembert method and computer algebra were utilized to obtain symbolic results for a conical rod falling on rigid ground to investigate the effect of the geometric shape of the rod (Hu *et al.* 2001). The Mode superposition method was considered to obtain the response of conical rods to longitudinal impact for fixed-free and free-free boundary conditions (Bao and Deng 2006). This analysis was extended to free-elastic boundary conditions by considering a conical rod with a supporting spring (Bao and Deng 2007). An approximate analytical method, specifically the Fourier series, had been used to specify the response of an abutment to longitudinal impact. The abutment has a conical shape, and it has equipment installed at its upper end (Ulitin and Tsarenko 2015). Velocity and stress distribution due to longitudinal impact waves in variable cross-section rods were obtained using the D'Alembert method, and the analysis showed that the change rate of the cross-section has a significant influence on them (Jiao and Ma 2016). Averaging variable coefficients had been utilized to model the longitudinal impact on variable section rods (Ulitin and Tsarenko 2016). The case of a rod with variable cross-section subjected to longitudinal impact had been solved using the Fourier series in Bessel functions (Stepanov *et al.* 2018, Ulitin and Tsarenko 2018).

In many applications, the wave propagates through the axial bodies while they are not fixed, as in hammering. In other applications, the elasticity of the foundation must be considered as in the driving of piles in the soil and percussive drilling in mining. The longitudinal impact of an elastic rod that is elastically fixed at one end and is hit by a mass at its other end represents the real settings when a stamping device used in forging is hit by a large block. Hence, not only fixed boundary conditions at the far end of the bar must be counted, but also free and elastic conditions.

However, it is unambiguous that the analytical solutions for the impact-induced stress waves in non-uniform rods are inadequate; for instance, none is available for a rod of complex configuration (Stepanov *et al.* 2018). Since the finite element method is accurate and efficient, it has been successfully applied to investigate the longitudinal impact of uniform rods with effects of various support conditions (Ramírez and Rubio-Gonzalez 2006, Elkaranshawy and Bajaba 2008, Idesman *et al.* 2010, Elkaranshawy and Bajaba 2012, Ragab and Fayed 2018, Etiwa *et al.* 2021, Etiwa and Elkaranshawy 2022, Etiwa *et al.* 2023), stress waves in a damaged rod subjected to longitudinal impact (Bajaba and Elkaranshawy 2008, Elkaranshawy 2019, Kumar *et al.* 2017), and the longitudinal vibration of variable cross-section rods (Gan *et al.* 2016, Hull 2018). Therefore, reliable finite element models are importantly required for the analysis of the impact on variable cross-section rods. The aim of this study is to use the finite element method to analyze the impact problem of variable cross-section rods colliding with a rigid mass. The formulation is developed based on St. Venant's contact theory. The influence of boundary conditions, mass ratios, and the geometrical shape of the rod on contact forces, displacements, velocities, and stresses are fully analyzed by illustrative examples. The struck mass and the rod are treated as an integrated system during the impact period, which eliminates discontinuities at the contact end and gives highly accurate results. The impact-induced stress

wave propagation in a fixed-free conical rod is investigated. The finite element results are verified by comparing them with analytical solutions of the mode of superposition method, and almost identical results are recognized. Also, the longitudinal impact waves in a conical rod with free ends and a conical rod attached to a spring are thoroughly investigated with illustrative examples.

It can be noticed that the literature primarily emphasizes approximate analytical solutions for specific cases of variable cross-section rods colliding with a rigid mass. In contrast, this study develops a finite element code to address the problem under various boundary conditions. The analysis focuses on understanding the physical phenomena of impact and wave propagation, including wave reflection at free, fixed, or spring-attached ends. The outcomes of this investigation improve our perception of this involved physical phenomenon. The results confirm the effectiveness of the finite element method and highlight its potential for application to more complex shapes and configurations, particularly in cases where analytical solutions are unavailable. The formulation presented can be used in modeling many applications mentioned before to validate the approximate analytical results, as benchmark templates used for crack detection, and can be extended to broader purposes in the field.

2. Mathematical modeling of longitudinal impact

2.1 Material and geometric properties

A homogeneous and linearly elastic conical rod is considered. It has Young's modulus E, density ρ, cross-section area $A(x)$, length L and mass m_{rod} The rod struck on the right end $(x = L)$ at time $t = 0$ by a moving rigid mass M_p of mass ratio $\gamma = m_{rod} / M_p$ and initial velocity v_o. The radius of the cross-section of the conical rod is variable (see Fig. 1(b)), and the radius at distance x from the left end of the rod is denoted by $r(x)$. The abbreviations: $a = \sqrt{\pi}\ (r(L) - r(0))/L$, $b = \sqrt{\pi}\ r(0)$ are used. Hence, the radius of the rod at distance x is $r(x) = (ax + b)/\sqrt{\pi}$ and the cross-sectional area of the rod at distance x is given by $A(x) = (ax + b)^2$. The area A_0 of the right section can be obtained as $A_0 = (aL + b)^2$

2.2 Governing equation of motion

The axial displacement and stress in a conical rod at position x and time t are denoted by $u(x,t)$ and $\sigma(x,t)$ respectively. The following relations are used for the velocity

$$v(x,t) = \dot{u}(x,t) = \partial u(x,t)/\partial t \tag{1}$$

and the strain

$$\varepsilon(x,t) = \partial u(x,t)/\partial x \tag{2}$$

The material is described by Hooke's law for linear elasticity

$$\sigma(x,t) = E\varepsilon(x,t) \tag{3}$$

It is assumed that the transverse waves of the rod and vibrations of the striking mass can be neglected. The contact surface is supposed to be perfectly planar so that St. Venant's contact theory can be used. According to these assumptions, the governing equation for the impact-induced wave of the rod is

$$\partial(\mathrm{EA}(x)\,\partial u/\partial x)/\partial x = \rho \mathrm{A}(x)\,\partial^2 u/\partial t^2, \quad 0 \le x \le L \tag{4}$$

or

$$\partial(\mathrm{A}(x)\,\partial u/\partial x)/\partial x = (\mathrm{A}(x)/{c_o}^2)\ \partial^2 u/\partial t^2, \quad 0 \le x \le L \tag{5}$$

where material-parameter $c_o = \sqrt{(E\ /\ \rho)}$ is the wave propagation velocity of the infinitesimal elastic pulse in the rod.

2.3 Boundary conditions

The boundary conditions for the unimpacted side of the rod $(\mathrm{x} = 0)$ for the three cases presented in Fig. 1(a), 2(a) and 2(b) are

$$\begin{cases} u(0,t) = 0, & \text{fixed (no displacement)} \\ \partial u(0,t)/\partial x = 0, & \text{free (no stress)} \\ A(0)E\,\partial u(0,t)/\partial x = ku(0,t) & \text{attached to a spring} \end{cases} \tag{6}$$

where k is the stiffness of the spring.

The rigid mass remains in contact with the rod if the contact force is compressive. The boundary conditions at the contact of the rod $(x = L)$ are given as follows

$$EA_o\ \partial u(L,t)/\partial x = -M_p\,\partial^2 u(L,t)/\partial t^2, \quad 0 < t \le t_c \tag{7}$$

Analytical where t_c is the time for contact duration, after which the rigid mass is no longer in contact with the rod, and the rod performs free vibration without the mass at the tip. Hence

$$EA_o\,\partial u(L,t)/\partial x = 0 \qquad t > t\_c \tag{8}$$

2.4 The initial conditions

According to St. Venant's contact theory, once the impact occurs, the velocity of the struck end of the rod becomes immediately equal to the velocity of the rigid mass 〖v〗_o. Hence the initial conditions are

$$\begin{aligned} &u(x,0) = 0 && for && 0 \le x \le L \\ &\partial u(x,0)/\partial t = 0 && for && 0 \le x < L \\ &\partial u(x,0)/\partial t = -v_o && at && x = L \end{aligned} \tag{9}$$

Table 1 Longitudinal impact of a mass on a fixed-free conical rod (Bao and Deng 2006).

Items	Fixed-Free Conical Rod
Frequency equation	$\tan\lambda(\lambda/\alpha_o + (1-q)/\lambda) = 1$
Normal modes	$\phi_j(\xi) = \sin(\lambda_j \xi)/(\xi + s)$
Generalized mode mass	$\beta_j = (q^2/s^2)\left[(1/2 - \sin(2\lambda_j)/4\lambda_j)\alpha_o + \sin^2\lambda_j\right]$
Displacement $u(x,t) = -(v_o L/c_o)\tilde{u}(\xi,\tau)$	$\tilde{u}(\xi,\tau) = \sum_{j=1}^{\infty} \sin\lambda_j/\lambda_j\beta_j(1+s) \times \sin(\lambda_j\xi)/(\xi+s) \times \sin(\lambda_j\tau)$
Velocity $v(x,t) = -v_o\tilde{v}(\xi,\tau)$	$\tilde{v}(\xi,\tau) = \sum_{j=1}^{\infty} \sin\lambda_j/\beta_j(1+s) \times \sin(\lambda_j\xi)/(\xi+s) \times \cos(\lambda_j\tau)$
Internal Forces $p(x,t) = -(\mathrm{EA}v_o/c_o)\varepsilon(\xi,\tau)$	$\varepsilon(\xi,\tau) = -\sum_{j=1}^{\infty} \sin\lambda_j \sin(\lambda_j\tau)/\beta_j(1+s) \times \left(\cos(\lambda_j\xi)/(\xi+s) - \sin(\lambda_j\tau)/\lambda_j(\xi+s)^2\right)$

(a) (b)

Fig. 1 Longitudinal impact of a mass on a conical rod; (a) fixed-free rod and (b) shape and variables of the conical rod

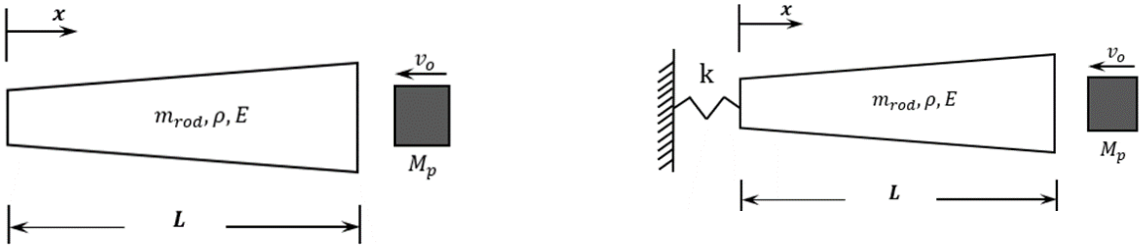

(a) (b)

Fig. 2 Longitudinal impact of a mass on a conical rod; (a) free-free rod and (b) rod with a spring

3. Solutions for the fixed-free rod

The analytical solution can be obtained using the mode superposition method, which is also called separation of variables technique. The solution of Eq. (4) is assumed to be a product of two functions, mode shape and frequency functions, each depending on only one of parameters *x* and *t*.

The substitution in the partial differential equation Eq. (4) leads to two separate ordinary differential equations that replace the original Eq. (4). The ordinary differential equation for the mode shape functions can be solved by satisfying the boundary, given in subsection 2.3. Also, the ordinary differential equation for the frequencies can be solved by satisfying the initial conditions, given in subsection 2.4. Bao and Deng 2006 obtained the frequency equations and mode shape functions of the longitudinal vibrations of the continuous rod with various boundary conditions in the beginning. Then, they obtained the dynamic responses of the rod with a mass-attached system can by the superposition principle.

Let us first introduce the dimensionless space coordinate, time, and frequency of the the system: $\xi = x/L$, $\tau = tc_o/L$, $\lambda = \omega L/c_o$, and the parameters: $s = b/(aL)$, $q = b/(b+aL)$, $\alpha_o = 3\gamma/(1+q+q^2)$, where ω is the inherent vibration frequency and $\gamma = m_{rod}/M_p$ is the mass ratio of the rod to the striking mass. It should be noted that $\tau = 1$ is the dimensionless time required for a longitudinal

Table 2 Dimensionless frequencies of a fixed-free conical rod attached with a mass (Bao and Deng 2006)

Mode	$\gamma = 1$	$\gamma = 0.5$	$\gamma = 0.25$
1	0.8631454	0.6318729	0.4547486
2	3.2769783	3.2096680	3.1756803
3	6.3512824	6.3172758	6.3002358
4	9.4702186	9.4475103	9.4361456
5	12.6004618	12.5834212	12.5748965

wave to propagate from one end of the rod to the other end. Table 1 summarizes the equations of the analytical solution of the longitudinal impact between the rigid mass and the fixed-free conical rod shown in Fig. 1(a). The dimensionless displacement $\tilde{u}(\xi,\tau)$, velocity $\tilde{v}(\xi,\tau)$, and strain $\varepsilon(\xi,\tau)$ are functions of the dimensionless frequency (λ_j), position (ξ), and time (τ). For more details about the derivation of the analytical solution, refer to Bao and Deng (2006). Table 2 shows the first five dimensionless frequencies λ_j for a fixed-free conical rod attached with a mass for thtee different mass rations $\boldsymbol{\gamma}$, obtained using system's frequency equation for the case: $a=-0.5,\ b=1,$ and $L=1$. It can be noticed that the frequency value decreases when the striking mass increases.

4. Finite element solution

4.1 Equation of motion

The finite element formulation for the pre-mentioned wave equation (Eq. (5)) is derived by assuming that the domain of the problem is divided into finite elements. It is assumed in *each element* that

$$u(x,t)=N(x)U^e(t) \tag{10}$$

where the superscript e denotes the element vector, $N(x)$ denotes the shape function, and $U^e(t)$ is the vector of nodal displacement that is assumed to be a function of time t. Eq. (4) can be written for each element using the *Galerkin* method as

$$\int_{x_1^e}^{x_2^e} N^T(\rho A\,\partial^2u/\partial t^2-\partial(EA\,\partial u/\partial x)/\partial x)\mathrm{d}x=0 \tag{11}$$

where x_1^e and x_2^e are the global coordinates of the two end nodes of the element. Integrate Eq. (11) by parts gives

$$\begin{aligned}&\int_{x_1^e}^{x_2^e}(N^T\rho A\,\partial^2u/\partial t^2)\,dx\\&\quad+\int_{x_1^e}^{x_2^e}(dN^T/dx)EA(\partial u/\partial x)\,dx\\&\quad=N^TEA(\partial u/\partial x)|_{x_1^e}^{x_2^e}\end{aligned} \tag{12}$$

Utilizing Eq. (10) and its derivatives, Eq. (12) gives

$$\begin{aligned}&\left(\int_{x_1^e}^{x_2^e}(N^T\rho AN)\,dx\right)\ddot{U}^e\\&+\left(\int_{x_1^e}^{x_2^e}(dN^T/dx)EA(dN/dx)\,dx\right)U^e\\&=(N^TEA\,\partial u/\partial x)|_{x_1^e}^{x_2^e}\end{aligned} \tag{13}$$

The rod is divided into $(n-1)$ linear elements, which gives (n) global nodes. For linear elements, the shape functions are

$$N(x)=[N_1\quad N_2]=[(x_2^e-x)/l\quad(x-x_1^e)/l] \tag{14}$$

where l is the length of the element. Hence, Eq. (13) can be written as

$$[M^e]\ddot{U}^e+[K^e]U^e=\{R^e\} \tag{15}$$

where the element mass matrix $[M^e]$, the element stiffness matrix $[K^e]$, and the force vector $\{R^e\}$ are given by

$$[M^e]=\int_{x_1^e}^{x_2^e}(N^T\rho AN)\,dx=(\rho A^el/6)\begin{bmatrix}2&1\\1&2\end{bmatrix} \tag{16}$$

$$\begin{aligned}[K^e]&=\int_{x_1^e}^{x_2^e}(dN^T/dx)EA(dN/dx)\,dx\\&=(EA^e/l)\begin{bmatrix}1&-1\\-1&1\end{bmatrix}\end{aligned} \tag{17}$$

$$\{R^e\}=(N^TEA\,\partial u/\partial x)|_{x_1^e}^{x_2^e}=\begin{Bmatrix}-EA^e\,\partial u/\partial x|_{x_1^e}\\EA^e\,\partial u/\partial x|_{x_2^e}\end{Bmatrix} \tag{18}$$

The cross-sectional area of each element is approximated to be constant and has the value $A^e=(A_i+A_{i+1})/2$, where $i=1,2,\ldots,n$ and it refers to the node index. The right side of Eq. (18) indicates that $\{R^e\}$ simply represents the nodal forces since $EA^e\,\partial u/\partial x=\sigma A^e=$ nodal force.

4.2 Boundary conditions

The rod could have fixed, free, or elastic boundary conditions at $x=0$, as follows.

$$\begin{cases}U_1=0 & \text{rigid}\\R_1=0 & \text{free}\\R_1=-kU_1 & \text{elastic}\end{cases} \tag{19}$$

The boundary conditions at the contact end $x=L$ during impact and after the cease of impact are

$$\begin{aligned}R_n&=-M_p\ddot{U}_n & 0<t<t_c\\R_n&=0 & t>t_c\end{aligned} \tag{20}$$

All element matrices are assembled into the global system, and the boundary conditions are applied. The resulting finite element equation is a coupled system of second-order differential equations in time of the form

$$[M]\{\ddot{U}\}+[K]\{U\}=\{R\} \tag{21}$$

where and $\{U\}$ and $\{\ddot{U}\}$ are the displacement and acceleration vectors, and $[M]$ and $[K]$ are the mass and the stiffness matrices, $\{R\}$ is the nodal force vector which in effect is nothing but the nodal reaction force vector.

4.3 Initial conditions

The initial conditions are

Table 3 Step-by-step solution using the Newmark integration method (Ragab and Fayed 2018, Bathe 2014).

A. Initial calculation

1. Form stiffness matrix $[K]$ and mass matrix $[M]$, during the contact period, the mass matrix is modified by replacing $M_{n\times n}$ by $M_{n\times n}+M_p$.
2. Initialize $\{U_o\}, \{\dot{U}_o\}$, and $\{\ddot{U}_o\}$
3. Select time step Δt and parameters α and δ and calculate integration constants:

$$\Delta t = (0.6-0.9)L/((\mathrm{n}-1)\,c_o)\,; \quad \delta \geq 0.50; \quad \alpha \geq 0.25(0.5+\delta)^2;$$
$$a_0 = 1/(\alpha\,\Delta t^2)\,; \quad a_1 = \delta/(\alpha\Delta t)\,; \quad a_2 = 1/(\alpha\Delta t)\,; \quad a_3 = (1/(2\alpha))-1\,;$$
$$a_4 = (\delta/\alpha)-1; \quad a_5 = (\Delta t/2)\big((\delta/\alpha)-2\big); \quad a_6 = \Delta t(1-\delta); \quad a_7 = \delta\Delta t;$$

Form effective stiffness matrix K_{eff}: $\left[K_{eff}\right] = [K] + a_0[M]$.

B. For each time step:

1. Calculate effective loads F at time $t+\Delta t$:
$$\{F^{t+\Delta t}\} = [M](a_0\{U^t\} + a_2\{\dot{U}^t\} + a_3\{\ddot{U}^t\})$$
2. Solve for displacement at time $t+\Delta t$:
$$\left[K_{eff}\right]\{U^{t+\Delta t}\} = \{F^{t+\Delta t}\}$$
3. Calculate acceleration and velocities at time $t+\Delta t$:
$$\{\ddot{U}^{t+\Delta t}\} = a_0\big(\{U^{t+\Delta t}\} - \{U^t\}\big) - a_2\{\dot{U}^t\} - a_3\{\ddot{U}^t\}$$
$$\{\dot{U}^{t+\Delta t}\} = \{\dot{U}^t\} + a_6\{\ddot{U}^t\} + a_7\{\ddot{U}^{t+\Delta t}\}$$
4. Calculate the secondary variable at time $t+\Delta t$:
$$\{R^{t+\Delta t}\} = [M]\{\ddot{U}^{t+\Delta t}\} + [K]\{U^{t+\Delta t}\}$$
5. Check the sign of the contact force R_n which must be negative during the contact period. The block loses contact with the rod tip when R_n becomes positive (tension)

Use the unmodified mass matrix to investigate the free vibration by applying the previous steps.

$$\begin{aligned} U_i &= 0 && \text{for} \quad i = 1,2,\dots,n \\ \dot{U}_i &= 0 \ \text{for} \ i = 1,2,\dots,n-1, \text{and} && \dot{U}_n = -v_o \\ \ddot{U}_i &= 0 && \text{for} \quad i = 1,2,\dots,n \end{aligned} \tag{22}$$

4.4 Procedure

A key point in the proposed finite element formulation is to consider the conical rod and the striking body as a rod with a mass attached during the impact period. Accordingly, during the impact period, the $n \times n$ term in the mass matrix is modified be $M_{n\times n} + M_p$, and the nodal reaction force at the contact point is $R_n = -M_p\ddot{U}_n$, as given in the first boundary condition in Eq. (20). During the duration of contact, the impact force, R_n, is always negative. Once it becomes positive (tension) in the progress of computation, it indicates the separation of the striking body from the conical rod, and the contact phase is complete. Hence, the nodal reaction force at the contact point is switched to $R_n = 0$, as given in the second boundary condition in Eq. (20), and the $n \times n$ term in the mass matrix is returned to its original value $M_{n\times n}$. As a result, the rod and the mass are treated separately. The displacement, velocity, and acceleration of the striking mass are the same as those of the impacted end as long as the R_n is negative. While the finite element method is used to discretize the space, the Newmark method is used for time integration (Ragab and Fayed 2018, Bathe 2014). The complete algorithm for the analysis of the longitudinal impact of rods using the Newmark integration scheme is given in Table 3.

5. Analysis and discussion

The effects of mass ratios on the stress wave propagation, contact force, deformation, and velocity of the conical rod are considered. The longitudinal impact of the conical rod with fixed, free, and deformable support conditions is simulated. Whenever an analytical solution is mentioned, it means the solutions are obtained with the direct mode superposition method. For the analytical solution, 4000 mode shapes are used. For the finite element analysis, the rod is divided into 500 linear elements, the fixed dimensionless time step is 1.5×10^{-3}, and the integral parameters of the Newmark method are $\alpha = 0.26$ and $\delta = 0.54$. The first global node is the left end at $x = 0$, and the impacted end is node $n = 501$ at $x = L$.

5.1 Longitudinal impact of fixed-free conical rod

This section presents the propagation of the longitudinal impact waves through the fixed-free conical rod illustrated in Fig. 1(a). The effects of mass ratio on the dynamic responses are thoroughly analyzed. The analytical solutions are obtained using the model superposition method (Bao and Deng 2006).

5.1.1 Propagation of the longitudinal impact wave

The propagation of impact-induced stress waves in the rod is visually displayed in Figs. 3 and 5. During impact, the striking body produces a compressive stress wave at the contact interface, which travels towards the fixed end with a characteristic velocity c_o. As shown in Figs. 3(a) and 3(b), the stress in the undisturbed regions equals zero until the

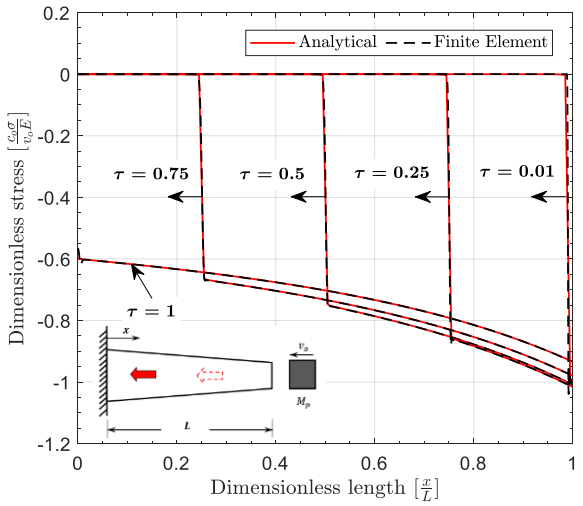

(a) $a = -0.4, b = 1, L = 1$

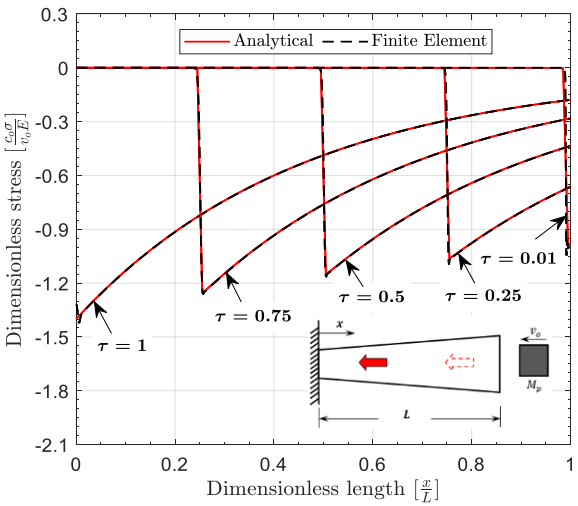

(b) $a = 0.4, b = 1, L = 1$

Fig. 2 Stress wave propagation in a conical rod struck longitudinally by a block for $\gamma = 1$ during the interval $\{0,\ L\ /\ c_o\}$

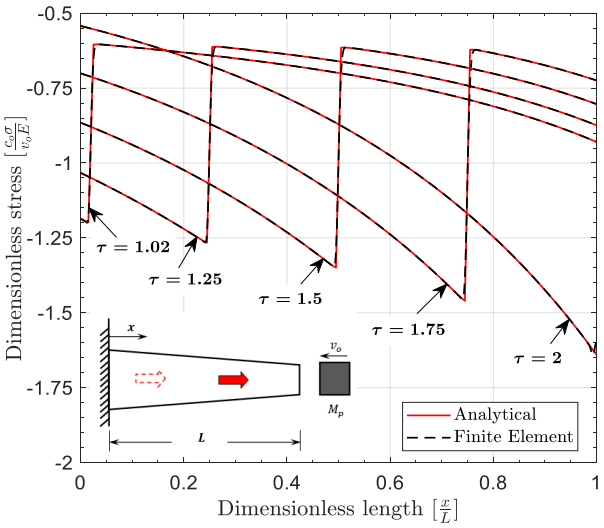

(a) $a = -0.4, b = 1, L = 1$

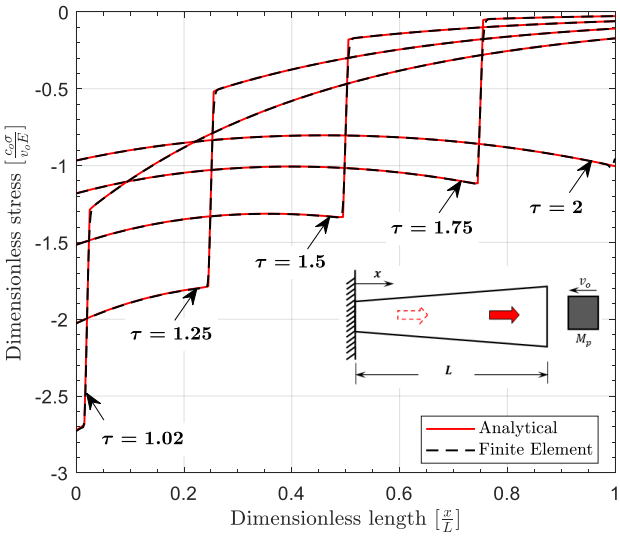

(b) $a = 0.4, b = 1, L = 1$

Fig. 3 Stress wave propagation in a fixed free rod struck longitudinally by a block for $\gamma = 1$ during the interval $\{L/c_o, 2\,L/c_o\}$

arrival of the incidence wave. The compressive stress wave is reflected from the fixed end as a compressive wave at time $\tau = 1$. The stresses of the reflected wave from the fixed end superimpose to give a double peak value, hence, double the value of the compressive stress is evident at $1 < \tau \leq 1.02$ as presented in Figs. 3 and 4. This stress multiplication phenomenon is characteristic of the fixed boundary. Along the rod, as the reflected wave reached any cross-section, the compression stress increases at that section. The discontinuity of the stress at any point marks the arrival of the wave at that point. During the contact period, the contact tip works as a fixed end, and the compressive wave is reflected from that end as a compressive wave again at time $\tau = 2$ with a double peak value. Hence, several reflections of the stress wave as a compressive wave occurs during the contact period. The wave reflects and transmits as a compressive wave from the fixed end and the contact tip until the contact terminates. So, the whole rod is under compression during the contact period. Also, the arrival of the reflected compression wave to the contact end raises the stress at the contact end, as shown in Figs. 5(a) and 5(b). After the cease of impact at the time t_c , the rigid mass is no longer in contact with the rod, and the rod performs free oscillations without the mass at the tip. The rod-free tip reflects the stress wave with opposite polarity. The analytical results are obtained according to the formula in. Excellent agreement between the finite element solutions and the analytical solutions is found.

When the taper is positive, the stress in the rod varies with space coordinate and follows the same pattern as the uniform rod considered in (Etiwa *et al.* 2021, 2023). However, the results show a different pattern when the taper is negative. As shown in Figs. 3(a) and 3(b), when $\tau \leq 1$, the taper affects the wave propagation, whereas the fixed boundary has no effect. It can be noticed in the same figure that if the taper is positive,

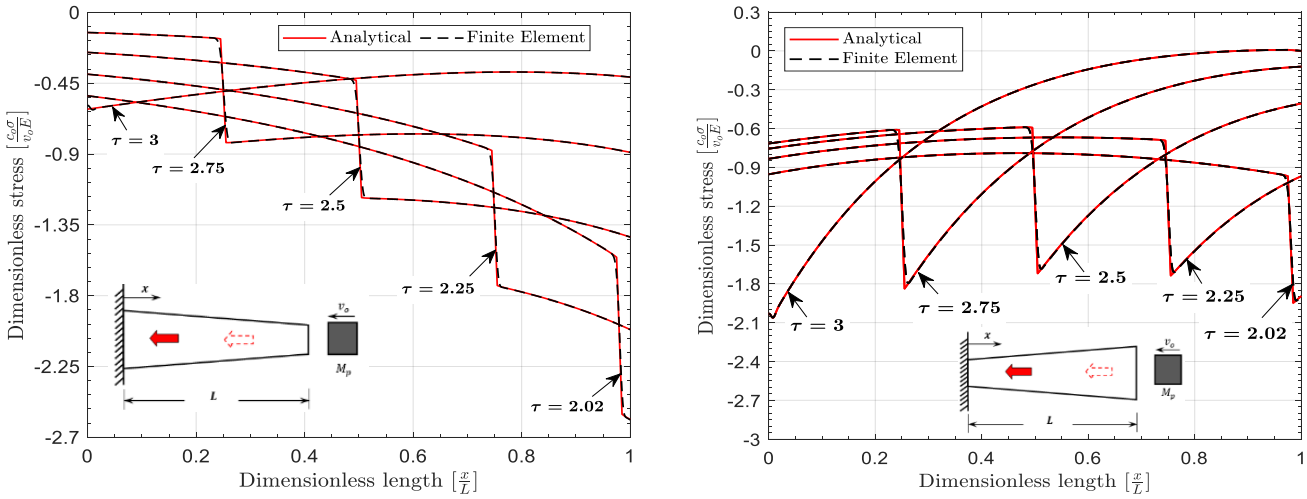

(a) $a = -0.4, b = 1, L = 1$ (b) $a = 0.4, b = 1, L = 1$

Fig. 4 Stress wave propagation in a fixed free rod struck longitudinally by a block for $\gamma = 1$ during the interval $\{2L/c_o, 3L/c_o\}$

Table 4 Comparison of amplitudes of incident wave for finite element and analytical solutions during interval $\{0, L/c_o\}$

Item	$x = 0.99L$	$x = 0.75L$	$x = 0.5L$	$x = 0.25L$	$x = 0$
	conical rod of $a = -0.4$				
Analytical	-0.9961	-0.8553	-0.74788	-0.66444	-0.59998
Finite Element	-1.0088	-0.86191	-0.75277	-0.66786	-0.58869
Error %	1.2749	0.772125	0.653445	0.514268	1.88255
	conical rod of $a = 0.4$				
Analytical	-0.9865	-1.0609	-1.1491	-1.2532	-1.3999
Finite Element	-1.02247	-1.07434	-1.15757	-1.25534	-1.3681
Error %	3.64622	1.26684	0.73709	0.170762	2.27159

Table 5 Comparison of amplitudes of reflected wave for finite element and analytical solutions during interval $\{L/c_o, 2L/c_o\}$

Item	$x = 0.02L$	$x = 0.25L$	$x = 0.5L$	$x = 0.75L$	$x = L$
	conical rod of $a = -0.4$				
Analytical	-1.19763	-1.26595	-1.34942	-1.46009	-1.640
Finite Element	-1.19882	-1.2669	-1.34954	-1.45856	-1.61798
Error %	0.09936	0.07504	0.00889	0.10478	1.34268
	conical rod of $a = 0.4$				
Analytical	-2.6859	-1.78533	-1.33444	-1.11543	-1.0
Finite Element	-2.6987	-1.79325	-1.33904	-1.11711	-0.98807
Error %	0.47656	0.44361	0.34471	0.15061	1.1930

the maximum value for the compression stress at the front of the wave increases as the wave moves toward the fixed end. Contrary to that, for the wave in the rod with negative tapered, the maximum value for the compression stress at the front of the wave decreases as the wave moves towards the fixed end.

When the wave reaches the fixed end at $\tau = 1$, for the rod with positive tapered, the absolute value of the dimensionless stress is greater than one. Opposite to that, when the wave reaches the fixed end, for the rod with negative tapered, the absolute value of the dimensionless stress is less than one. As shown in Figs. 4(a) and 4(b), the stresses of the reflected wave from the fixed end superimpose to give a double peak value at the fixed end. As the reflected wave reaches any cross-section,

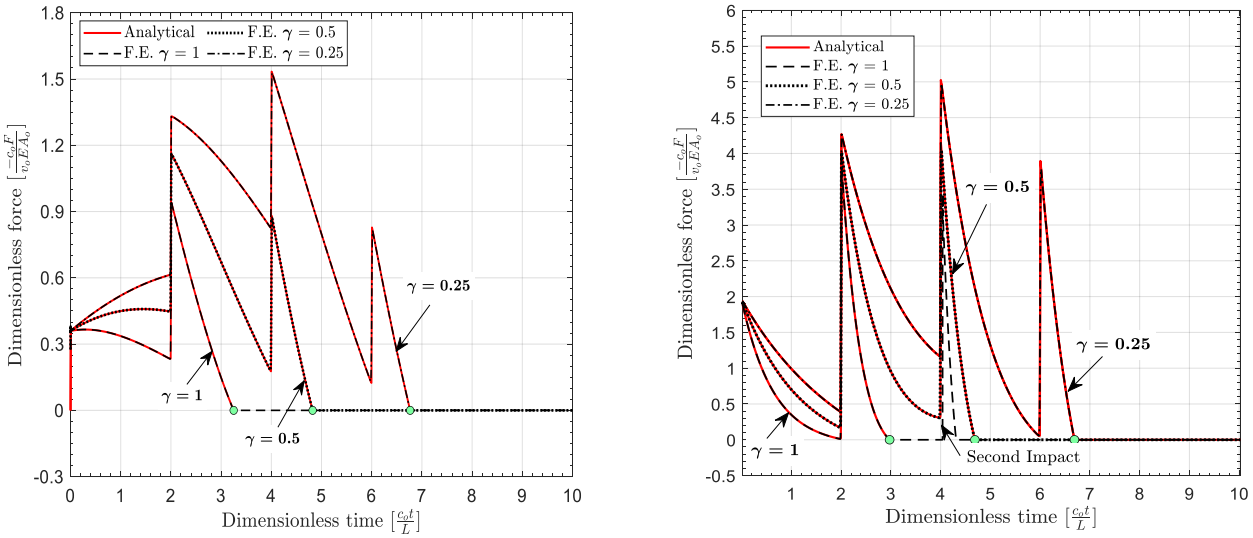

(a) $a = -0.4, b = 1, L = 1$ (b) $a = 0.4, b = 1, L = 1$

Fig. 6 Dimensionless contact force between a fixed-free conical rod and a striking mass for three mass ratios

the compression stress increases at that section. For the positive tapered, the increase in the value of the stress at the front of the wave decreases as the reflected wave moves from the fixed end toward the contact end. For the negative tapered, the increase in the value of the stress at the front of the wave increases as the reflected wave moves from the fixed end toward the contact end. Hence, the wave prorogation is affected by both the taper and the fixed boundary of the rod. Accordingly, it can be concluded that the impact behavior of conical rods is more complicated than that of uniform rods. Table 4 presents the amplitudes of incident stress wave during the interval $\{0, L/c_o\}$ for both cases of the conical rods with $a = -0.4$ and $a = 0.4$. Table 5 presents the amplitudes of reflected stress wave from the fixed end during the interval $\{L/c_o, 2\,L/c_o\}$ for both cases of the conical rods with $a = -0.4$ and $a = 0.4$. The two tables display both the analytical and finite element solutions at various positions along the rod. The percentage error of the finite element solution relative to the analytical solution is calculated according to

$$Error\ \% = \frac{|\sigma_{FE} - \sigma_{Analytical}|}{|\sigma_{Analytical}|} \times 100 \qquad (23)$$

where σ_{FE} and $\sigma_{Analytical}$ represent the amplitudes of the dimensionless stresses obtained from the finite element analysis and the analytical solutions, respectively. It can be noticed that the error values are less than 1% except at the ends of the rod, where they range between 1.19% and 3.65%. The table demonstrates that the proposed finite element solution precisely captures this complex phenomenon.

5.1.2 Effects of mass ratio

Fig. 7 shows the time history of the dimensionless stress at the quarter positions of the conical rod during the contact duration and after the cease of impact for three mass ratios $\gamma = 1, 0.5, \text{and } 0.25$. The propagation of waves is described by the lines $c_o t \pm x \pm 2iL = 0, i = 0, 1, 2, 3, \ldots$ whose arrival at any location produces a sudden stress jump. The undisturbed regions have no stress until the waves have arrived, and the stress of the section where the incident waves have already passed increases correspondingly. The arrival reach their maximum value at the first reflection $\tau = 2$ for $\gamma = 1$ and 0.5, and at the second reflection $\tau = 4$ for $\gamma = 0.25$ as shown in Figs. 6 and 7. For the positive tapered, the rod tip strikes the rigid mass after the first contact-separation process for $\gamma = 1$, as presented in Fig. 6(b), this is called the "Succession collisions" phenomenon.

The finite element results agree with the analytical results very well. After the contact ceases at the time t_c, the rigid mass is no longer in contact with the rod, and the rod performs free oscillations. Since no analytical solution is available for $t > t_c$, only the finite element method is used to simulate the dynamic responses of the free oscillations of the rod after the cease of impact. In the free oscillation, the stress at the free end is always zero. Therefore, the rod-free tip reflects the stress wave with opposite polarity. Therefore, a part of the fixed free rod is in compression while the other part is in tension. Table 6 shows the dimensionless contact time and maximum dimensionless contact force for three of the reflected compression wave to the contact end raises the stress at the contact end. Accordingly, the contact forces mass ratios $\gamma = 1, 0.5, \text{and } 0.25$.

To demonstrate the mutual influences of mass ratios, wave propagation, and impact responses along the rod, we present the time histories of the main variables. Figs. 8 and 9 show the time history of the displacements and velocities at the contact end and at the quarter positions of the conical rod during the contact duration and after the separation of contact for the three mass ratios $\gamma = 1, 0.5, \text{and } 0.25$. The analytical solution is valid for $t \le t_c$, the finite element method is used to simulate the dynamic responses of the

Table 6 Dimensionless contact time and maximum dimensionless contact force for impact between fixed-free rod and rigid mass, $a = 0.4, b = 1, L = 1$

γ	Dimensionless contact time		Maximum dimensionless contact force	
	FEM	Analytical	FEM	Analytical
1	2.9800	2.9755	3.8546	3.8081
0.5	4.6900	4.6890	4.1489	4.0470
0.25	6.6900	6.6900	5.0254	4.9730

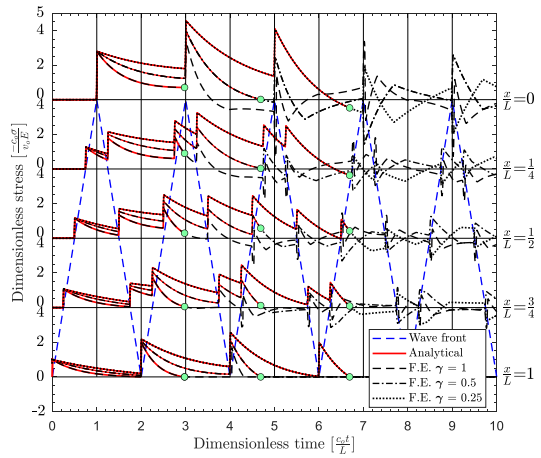

Fig. 5 Dimensionless stresses of a fixed-free conical rod struck longitudinally by a rigid mass for various mass ratios $\gamma = 1, 0.5,$ and 0.25 for $a = 0.4, b = 1, L = 1$

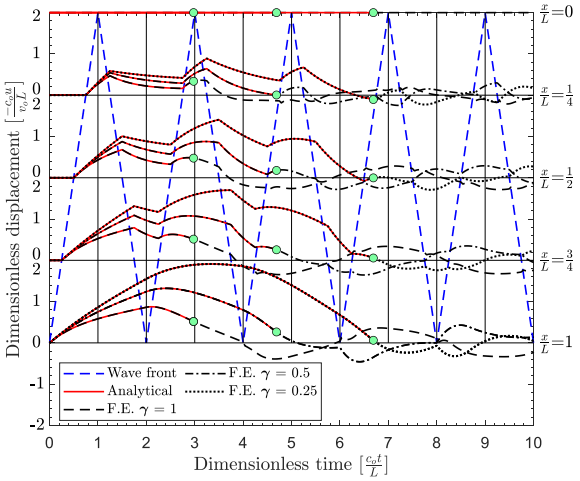

Fig. 6 Dimensionless displacements of a fixed-free conical rod struck longitudinally by a rigid mass for mass ratios $\gamma = 1, 0.5,$ and $0.25,$ and $a = 0.4$, $b = 1, L = 1$

free oscillations of the rod after the cease of impact. The propagation of waves is described by the lines $c_o t \pm x \pm 2iL = 0, i = 0, 1, 2, 3, \ldots,$, whose arrival at any location produces a discontinuity in the slope of the displacement histories corresponding to the sudden stress and velocity jumps described previously. The deformation of the section of the rod that the stress waves have already passed increases correspondingly, and the undisturbed regions show no deformation until the waves have arrived. The compressive stress wave, which travels through the rod, is reflected from the fixed end as a compressive wave at time $\tau = 1$. After $\tau = 1$, the compressive stress waves consecutively reach the boundary and simultaneously generate a continuous series of reflected waves that travel in the opposite direction to that of the original waves. During the contact period, the interaction of the reflected waves and the original compressive waves reduces the deformation of the interactive region and changes the direction of motion of that region.

The displacement at any point of the bar is continuous, but the velocity at the same point suffers discontinuities that correspond to the arrival of the stress wave. Table 7 shows the maximum dimensionless displacement of the contact end and the dimensionless rebound velocity for three mass ratios $\gamma = 1, 0.5,$ and 0.25 . Finite element results agree very well with analytical results.

To illustrate the harmony between the displacement at the contact end, the displacement of the rigid mass, and the contact force, the variation of all of these quantities are shown concurrently in Fig. 10, for the case when $\gamma = 0.25$. The contact end of the rod and the rigid mass have the same displacement during the first contact period. After the cease of impact, the striking mass moves in the positive x-axis with a constant velocity equal to the rebound velocity.

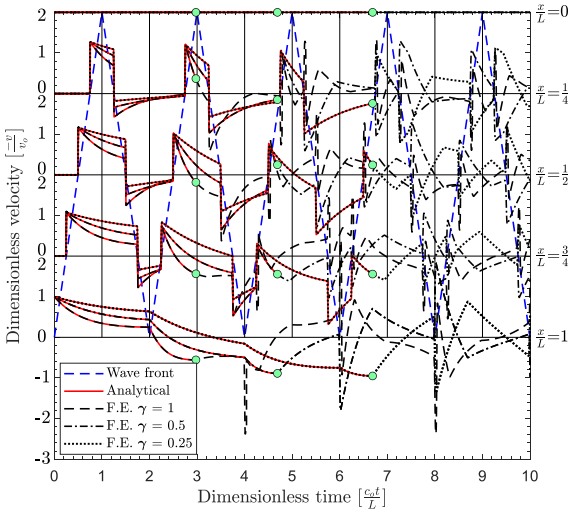

Fig. 7 Dimensionless velocities in a fixed-free conical rod struck longitudinally by a rigid mass for various mass ratios $\gamma = 1, 0.5,$ and 0.25 for $a = 0.4, b = 1, L = 1$

Table 7 Maximum dimensionless displacement at contact end and rebound velocity for impact between fixed-free conical rod and rigid mass, $a = 0.4, b = 1, L = 1$

γ	Maximum dimensionless displacement		Dimensionless rebound velocity	
	Analytical	FEM	Analytical	FEM
1	0.8756	0.8760	−0.5547	−0.5549
0.5	1.3209	1.3212	−0.8870	−0.8872
0.25	1.9109	1.9111	−0.9503	−0.9504

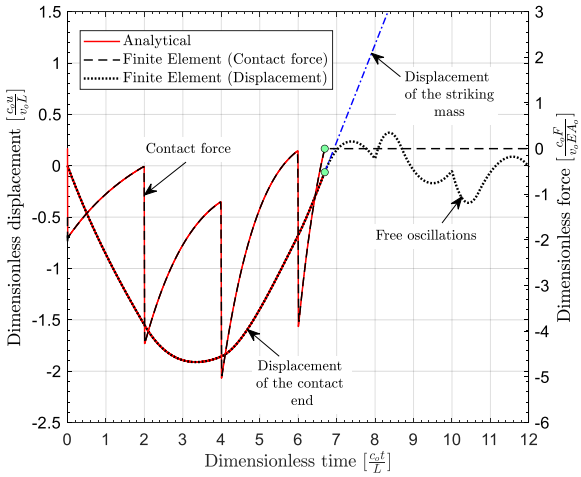

Fig. 8 Contact force, displacement of contact end, and displacement of the rigid mass for a fixed-free conical rod struck longitudinally by a rigid mass during and after the cease of impact; $\gamma = 0.25, a = 0.4, b = 1, L = 1$

5.2 Longitudinal impact of free-free conical rod

In this section, the propagation of the impact-induced stress waves through the free-free conical rod illustrated in Fig. 2(a) is presented. Also, the effects of the mass ratio and the geometrical shape of the rod on the dynamic response are analyzed.

5.2.1 Propagation of the longitudinal impact waves

A visualization of the propagation of impact-induced stress waves in the free-free conical rod is shown in Figs. 3 and 11. The compressive stress wave generated at the struck end at the instant of impact propagates along the rod at the characteristic velocity c_o. The stress of the section on the rod that the stress wave has already passed increases correspondingly, while the undisturbed region has no stress until the wave has arrived, as shown in Figs. 3(a) and 3(b). Furthermore, for $\tau < 1$, the taper affects the wave propagation, whereas the free boundary has no effect. When

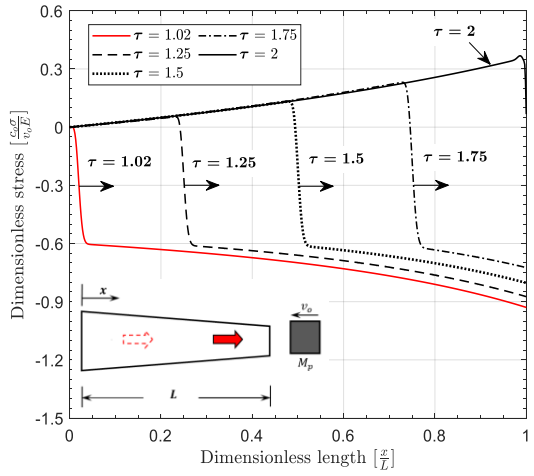

(a) $a = -0.4, b = 1, L = 1$

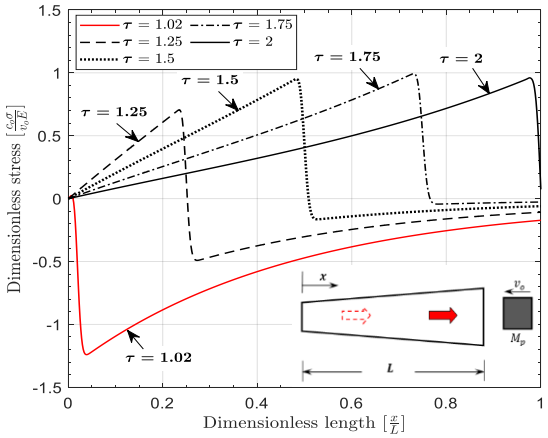

(b) $a = 0.4, b = 1, L = 1$

Fig. 9 Stress wave propagation of a free-free rod struck longitudinally by a block of mass ratio $\gamma = 1$ during the interval $\{L/c_o, 2\,L/c_o\}$

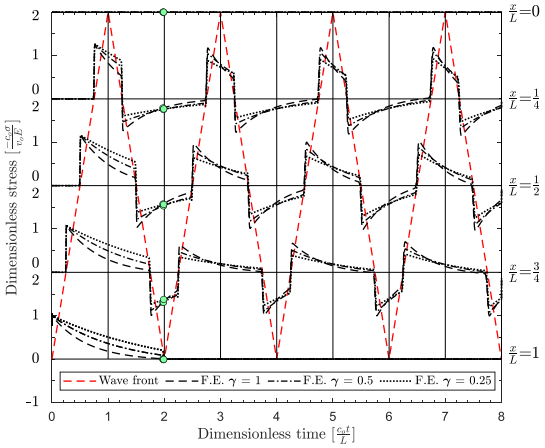

Fig. 10 Finite element results for dimensionless stresses of a free-free conical rod struck longitudinally by a rigid mass for $\gamma = 1, 0.5,\ 0.25$, and $a = 0.4, b = 1, L = 1$

the incident compression wave reaches the free end, it is reflected as a tension wave. This stress reversal is a characteristic of the free boundary. The reflected tension wave (or the rod's stress) is affected by both the taper and the free boundary of the rod. For $\tau > 1$, a part of the rod is in tension while the other part is in compression, as shown in Fig. 9(a) and 11(b). Therefore, the alternation of the stress at any point between compression and tension marks the arrival of the wave at that point. When the tension wave reaches the contact end, it cancels the stress to zero, and contact is terminated. So, the separation occurs at the same time $2L\ /\ c_o$. After the cease of impact, the right end of the rod will be free, and the rod will perform free oscillation. After separation, the stress at the two ends of the rod equals zero, and each end reflects the stress with opposite polarity. As shown in Figs. 3(a) and 3(b), when $\tau \leq 1$, the taper affects the wave propagation, whereas the free boundary has no effect. It can be noticed that if the taper is positive, the maximum value for the compression stress at the front of the wave increases as the wave moves towards the free end, and when it reaches the free end at $\tau = 1$, the absolute

value of the dimensionless stress is greater than one. Contrary to that, for the wave in the rod with negative tapered, the maximum value for the compression stress at the front of the wave decreases as the wave moves towards the free end, and when it reaches the free end, the absolute value of the dimensionless stress is less than one. As shown in Figs. 11(a) and 11(b), the incident compression wave is reflected at the free end as a tension wave. As the reflected tension wave reaches any cross-section, the stress at that section alternates from compression to tension. For the positive tapered, the jump in the value of the stress at the front of the wave decreases as the reflected wave moves from the free end toward the contact end. For the negative tapered, the jump in the value of the stress at the front of the wave increases as the reflected wave moves from the free end toward the contact end. Therefore, wave prorogation is affected by both the taper and the free boundary of the rod. Hence, it is ascertained that the impact behavior of conical rods is more complicated than that of uniform rods.

5.2.2 Effects of mass ratio

Fig. 12 shows the time history of the dimensionless stresses at quarter positions of the rod during the contact and after the cease of impact for three mass ratios, $\gamma = 1, 0.5,$ and 0.25. The propagation of waves is described by

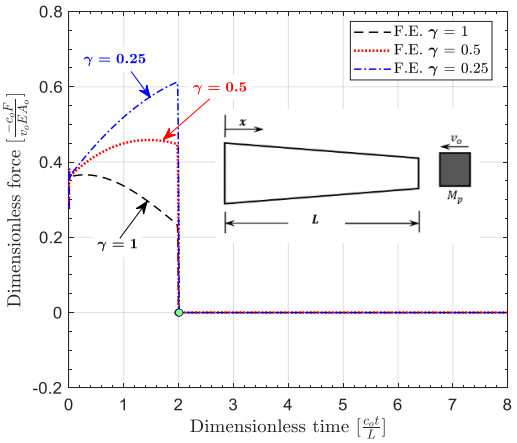

(a) $a = -0.4, b = 1, L = 1$

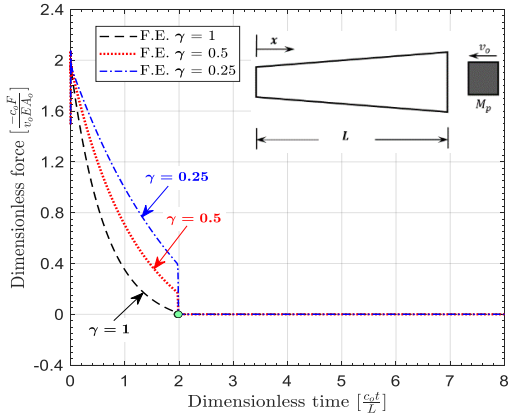

(b) $a = 0.4, b = 1, L = 1$

Fig. 12 Dimensionless contact force for a free-free conical rod struck longitudinally by a rigid mass for three mass ratios

The lines $c_o t \pm x \pm 2iL = 0, i = 0, 1, 2, 3, \ldots$, whose arrival at any location produces a sudden stress jump. The undisturbed regions have no stress until the wave has arrived, and the stress of the section of the rod that the incident wave has already passed increases correspondingly. The wavefront consecutively reaches the free end of the rod

Table 8 Dimensionless contact time and dimensionless rebo und velocity for impact between a free-free conical rod and a rigid mass, $a = 0.4, b = 1, L = 1$

γ	Dimensionless contact duration time τ	Dimensionless rebound Velocity
1	2	0.2510
0.5	2	0.4381
0.25	2	0.6395

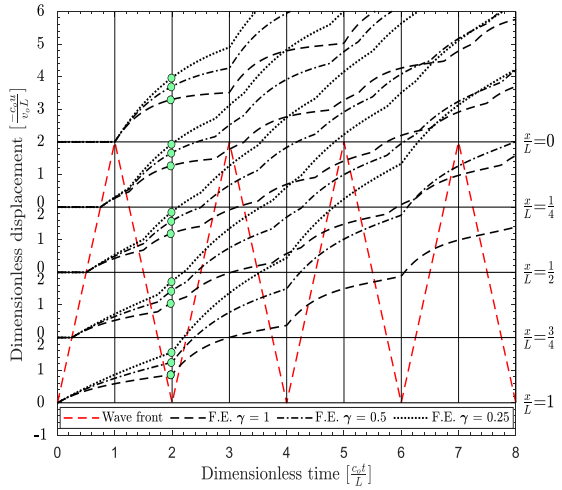

Fig. 13 Dimensionless displacements of a free-free conical rod struck longitudinally by a rigid mass obtained from the finite element solution for various mass ratios $\gamma = 1, 0.5,$ and 0.25 for $a = 0.4, b = 1,$ and $L = 1$

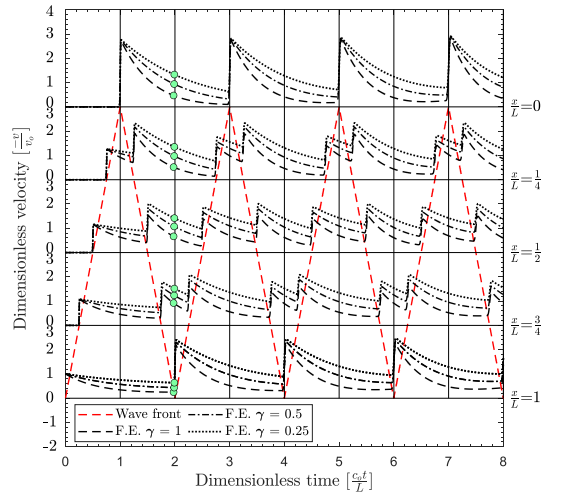

Fig. 14 Dimensionless velocities of a free-free conical rod struck longitudinally by a rigid mass obtained from the finite-element solution for various mass ratios $\gamma = 1, 0.5,$ and 0.25 for $a = 0.4, b = 1, L = 1$

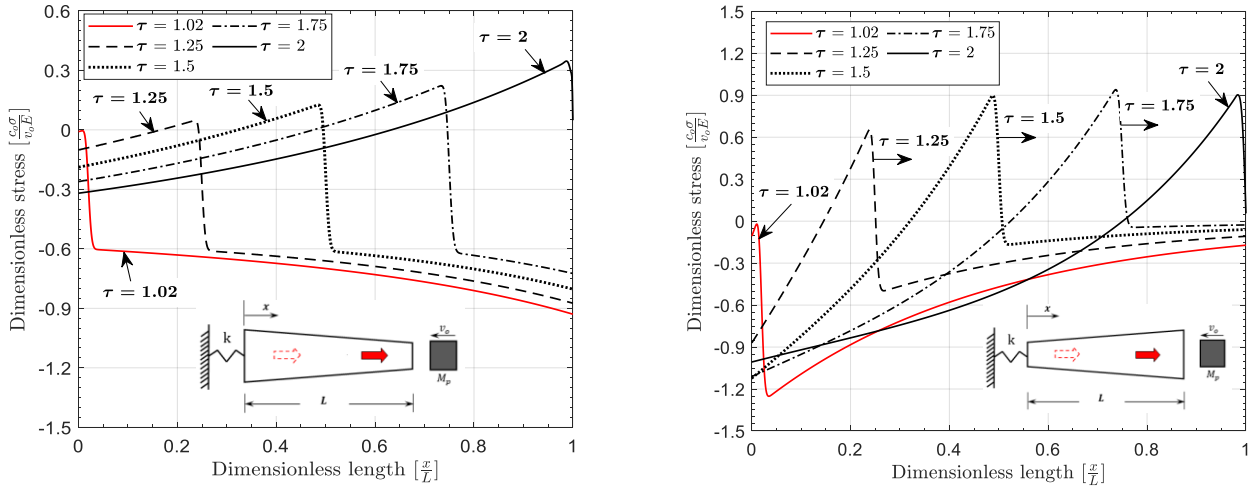

(a) $a = -0.4, b = 1, L = 1$ (b) $a = 0.4, b = 1, L = 1$

Fig. 16 Stress wave propagation for a rod attached to a spring of $k = k_1$ and struck longitudinally by a block for $\gamma = 1$ during the interval $\{L/c_o, 2\,L/c_o\}$

at time $\tau = 1$, and simultaneously, the stress at that end is zero, which generates a tension reflection wave that travels in the direction opposite to that of the incident wave. The small circles on the curves indicate the termination of contact.

The small circles on the curves indicate the termination of contact. After the cease of impact, the rigid mass is no longer in contact with the rod, and the rod performs free oscillations without the mass at the tip. The stresses at the two free ends are always zero. Therefore, the rod-free tip reflects the stress wave with opposite polarity. Therefore, a part of the free-free rod is in tension while the other part is in compression.

Figs. 13(a) and 13(b) show the time history of the dimensionless contact force at the contact end of the rod during the contact and after the cease of impact for three mass ratios, $\gamma = 1, 0.5, \text{and } 0.25$, the effect of the geometrical shape on the contact forces are presented. The small circles on the curves indicate the termination of contact. It can be noticed that for the high mass ratio $\gamma = 1$, the contact force vanishes, and consequently, the contact ceases before the arrival of the reflected tension wave.

Fig. 14 shows the time histories of the displacements at quarter positions of the conical rod during the contact and after the separation for the three mass ratios $\gamma = 1, 0.5, \text{and } 0.25$. The propagation of waves is described by the lines $c_o t \pm x \pm 2iL = 0, i = 0, 1, 2, 3, \ldots$, whose arrival at any location produces a discontinuity in the slope of the displacement histories. However, the displacements themselves are continuous. The undisturbed regions show no deformation until the wave has arrived, and the deformation of the section of the rod that the wave has already passed increases correspondingly. The compressive wave, which travels through the rod, is reflected from the free end as a tension wave at time $\tau = 1$.

Fig. 15 shows the time histories of the velocities at the quarter positions of the rod during the contact and after the separation for the three mass ratios $\gamma = 1, 0.5, \text{and } 0.25$. A similar behavior to that of the displacement can be observed, however, while the displacement is continuous, the velocity suffers discontinuities corresponding to the arrival of the waves. Table 8 shows the dimensionless contact duration time and the dimensionless rebound velocity for impact between the rod and the rigid mass for three mass ratios $\gamma = 1, 0.5, \text{and } 0.25$.

5.3 Longitudinal impact of conical rod with a spring

In this section, the propagation of the longitudinal impact waves through the conical rod attached to a spring illustrated in Fig. 2(b) is presented. The effects of the stiffness of the spring on stress wave propagation and the dynamic responses of the rod are precisely analyzed. We considered three values for the stiffness of the spring (k); $k = 0.02\,k_1$, $k = 0.2\,k_1$, and $k = 100\,k_1$, where $k_1 = EA_o/L$.

5.3.1 Propagation of the longitudinal impact waves

The propagation of impact-induced stress waves in the conical rod with spring illustrated in Fig. 2(b) is simulated. The spring has $k = k_1$. The compression wave generated at the struck end at the instant of impact propagates along the rod at a characteristic velocity c_o. The wavefront arrives at the end attached to the spring at $\tau = 1$. The undisturbed region has no stress until the wave has arrived, as shown in Figs. 3(a) and 3(b) for $\tau < 1$. Due to the existence of the spring, the stress at that end will not be zero like in the case of the free end, and the incident compression wave is reflected as a tension wave for a small value of spring constant or a compression wave for a large value of spring constant, as will be discussed later in section 5.3.2.

For the considered cases in Figs. 16(a) and 16(b), the incident compression wave is reflected as a tension wave. Therefore, one part of the rod is in tension while the other

part is in compression, and the stress at any point on the rod alternates between compression and tension, which is marked by the arrival of the wave at that point. When the tension wave reaches the contact end, it cancels the stress to zero, and contact is terminated. So, the separation occurs at the time $2L/c_o$. Following the cease of contact, the rod with the spring performs free oscillation without the striking body at the impacted end, and the wave is reflected from that end as a compression wave. This stress reversal is a characteristic of the free boundary.

For $\tau \leq 1$, the taper affects the wave propagation, whereas the elastic boundary has no effect, as shown in Figs. 3(a) and 3(b). For $\tau > 1$, the wave in the rod with negative tapered, the maximum value for the compression stress at the front of the wave decreases as the wave moves towards the end with the spring, and when it reaches the end with the spring, the absolute value of the dimensionless stress is less than one. For the cases considered, the incident compression wave is reflected at the end with the spring as a tension wave, as shown in Figs. 16(a) and 16(b). As the reflected tension wave reaches any cross-section, the stress alternates at that section from compression to tension. For the positive tapered, the jump in the value of the stress at the front of the wave decreases as the reflected wave moves from the end with the spring towards the contact end. For the negative tapered, the jump in the value of the stress at the front of the wave increases as the reflected wave moves from the end with the spring towards the contact end. Hence, the wave prorogation is affected by both the taper and the elastic boundary of the rod. Once again, it is established that the impact behavior of conical rods is more complicated than that of uniform rods.

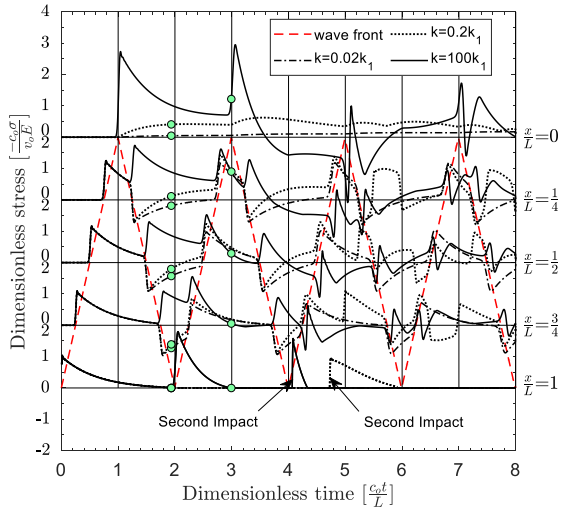

Fig. 15 Finite element results for dimensionless stresses of a conical rod attached to a spring and struck longitudinally by a rigid mass for three values of k and $\gamma = 1, a = 0.4, b = 1, L = 1$

5.3.2 Effects of the spring constant

To demonstrate the effects of the spring constant on the longitudinal oscillations of the conical rod, the time histories are presented. Figs. 17 - 19 show the variation of stresses, velocities, and displacements, respectively, at the quarter positions of the rod for values of $k = 0.02k_1, 0.2k_1,$ and $100k_1$. Until the arrival of the reflected wave, figures show that the displacements, velocities, and stresses are independent of the constraint on the left end $(x = 0)$. The small circles show the end of the impact. Due to the existence of spring, the stress at the end with the spring will not be zero like in the case of the free end.

The incident compression wave is reflected as a tension wave for the small value of the spring stiffness $k = 0.02k_1$ and $0.2k_1$, or a compression wave for the large value of the spring constant $k = 100k_1$, the rod tip strikes the rigid mass after the first contact-separation process for $k = 0.2k_1$ and $k = 100k_1$. After the cease of impact, the rod performs free oscillation, and the wave is reflected from the end without the spring with opposite polarity.

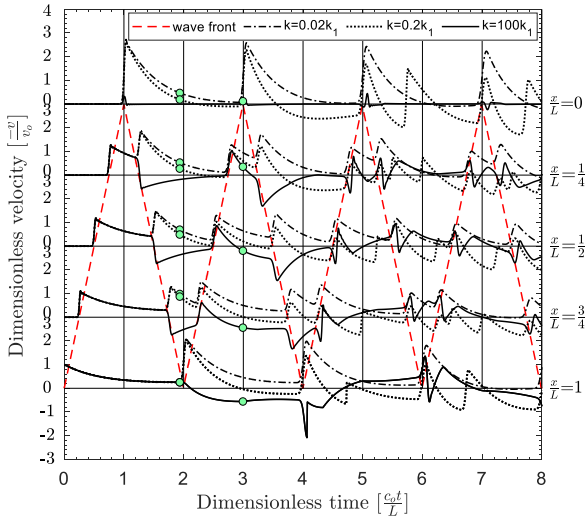

Fig. 16 Finite element results for dimensionless velocities of a conical rod attached to a spring and struck longitudinally by a rigid mass for three values of k and $\gamma = 1, a = 0.4, b = 1, L = 1$

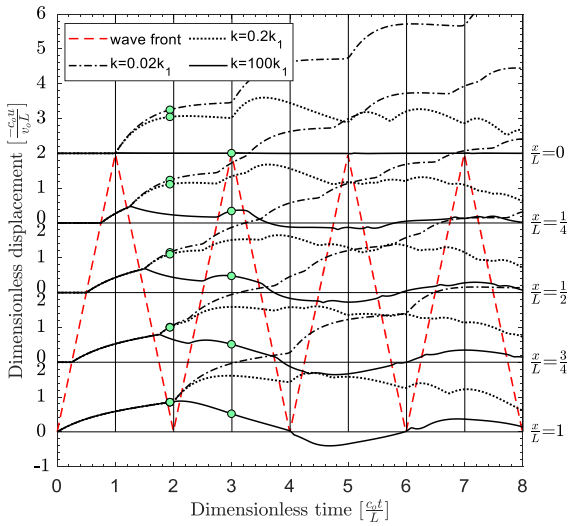

Fig. 19 Finite element results for dimensionless displacements of a conical rod attached to a spring and struck longitudinally by a rigid mass for three values of k and $\gamma = 1, a = 0.4, b = 1, L = 1$

6. Conclusions

A finite element formulation for the impact of a conical rod axially struck by a rigid mass has been presented. The dynamic response and the propagation of the impact-induced stress waves have been analyzed based on St. Venant's contact theory. The finite element analysis has been performed using the Newmark time integration method. When the impact wave arrives at the end of the rod, the traditional finite element codes suffer from inaccurate modeling of this discontinuity. The proposed model has solved this problem by modeling the struck mass and the rod as one system, which gives highly accurate outcomes. For the fixed, free, and elastic far end of the rod, results show the variation of contact forces, displacements, velocities, and stresses with respect to time. Impact peaks during the contact period have been shown in the impact force histories that were obtained. The effects of mass ratios, the boundary conditions, and the geometrical shape of the conical rod upon the rod dynamic response were presented. For instance, results show that the duration of contact is increasing with decreasing the mass ratio ($\gamma = m_{rod} / M_p$) for fixed-free rods. The change of the cross-section has a significant effect on the wave propagation in the rod during impact. If the cross-section area is decreasing, the discontinuous jump in the stress value at the front of the wave increases as the wave moves, while if the cross-section area is increasing, the jump in the stress value at the front of the wave decreases as the wave moves. In general, results show that the analysis of the variable cross-section rod is more complicated than that of the uniform rod. Excellent agreement has been found between the obtained numerical results and the analytical results of the mode of superposition method for a rod with a fixed unimpacted end. The presented visualization of stress, displacement, and velocity along the rod and stress wave propagation enhances the understanding of the physical phenomena of the propagation of impact-induced waves. The results confirm that the developed finite element technique effectively analyzes the collision of variable cross-section rod structures and provides a convenient, accurate, and applicable means to compute stress, displacement, velocity, and impact force histories.

References

Abdeddine, E., Majid, A., Beidouri, Z. and Zarbane, K. (2020), "Nonlinear longitudinal free vibration of uniform rods and rods with sections varying exponentially", In *XI International Conference on Structural Dynamics*, 239-251. https://doi.org/10.47964/1120.9019.19214.

Akbas, S.D. (2014), "Wave propagation analysis of edge cracked circular beams under impact force", *PloS one*, **9**(6), e100496. https://doi.org/10.1371/journal.pone.0100496.

Akbas, S.D. (2020), "Modal analysis of viscoelastic nanorods under an axially harmonic load", *Adv. Nano Res.*, **8**(4), 277-282. https://doi.org/10.12989/anr.2020.8.4.277.

Asiri, S.A., Akbas, S.D. and Eltaher, M.A. (2020), "Damped dynamic responses of a layered functionally graded thick beam under a pulse load", *Struct. Eng. Mech.*, **75**(6), 713-722. https://doi.org/10.12989/sem.2020.75.6.713.

Bajaba, N. and Elkaranshawy, H. (2008), "Damage detection in an elastic rod using finite element simulation to longitudinal impact waves", *Proceedings of the 15th International Congress on Sound and Vibration*, Daejeon, Korea, July.

Banerjee, J.R., Ananthapuvirajah, A. and Papkov S.O. (2020), "Dynamic stiffness matrix of a conical bar using the rayleigh-love theory with applications", *Eur. J. Mech - A Solids*, **83**, 104020. https://doi.org/10.1016/j.euromechsol.2020.104020.

Bao, S. and Deng, Z. (2006), "Analytical solutions for response of collision of particle with conical rod caused by longitudinal vibration", *Appl. Math. Mech.*, **27**(7), 927-934. https://doi.org/10.1007/s10483-006-0708-z.

Bao, S. and Deng, Z. (2007), "Analytical solutions of the impact problems of conical rod structures with a spring", *Acta Aeronautica Et Astronautica Sinica*, **28**(5), 1098-1103.

Bathe, K.J. (2014), *Finite element procedures*, (2nd Ed.), K.J. Bathe, Watertown, MA.

Bruno, D. and Randolph, M.F. (1999), "Dynamic and static load testing of model piles driven into dense sand", *J. Geotech. Geoenviron. Eng.*, **125**(11), 988-998. https://doi.org/10.1061/(ASCE)1090-0241(1999)125:11(988).

Chiang, L.E. and Elías, D.A. (2000), "Modeling impact in down-the-hole rock drilling", *Int. J. Rock Mech. Min. Sci.*, **37**(4), 599-613. https://doi.org/10.1016/S1365-1609(99)00124-0.

Dechao, Z. and Yufeng, X. (1996), "Analytical solution of point elastic impact between structures", *Acta Mechanica Sinica*, **28**(1), 99-103.

Elkaranshawy, H.A. (2019), "Stress waves in a damaged rod subjected to longitudinal impact", *Int. J. Mech. Eng. Robot. Res.*, **8**(3), 488-493. https://doi.org/10.18178/ijmerr.8.3.488-493.

Elkaranshawy, H.A. and Bajaba, N.S. (2008), "A finite element simulation to longitudinal impact waves in elastic rods", *Int. J. Appl. Eng. Res.*, **3**(6), 847-860.

Elkaranshawy, H.A. and Bajaba, N.S. (2012), "A finite element simulation of longitudinal impact waves in elastic rods", In *Materials with Complex Behaviour II*, (Eds., Andreas Öchsner, Lucas F. M. da Silva, and Holm Altenbach), 3-17. Springer.

Etiwa, R.M., Elabsy, H.M. and Elkaranshawy, H.A. (2023), "Dynamics of longitudinal impact in uniform and composite rods with effects of various support conditions", *Alexandria Eng. J.*, **65**, 1-22. https://doi.org/10.1016/j.aej.2022.09.050.

Etiwa, R.M. and Elkaranshawy, H.A. (2022), "Impact waves in a rod constrained by a stationary mass at one end and struck by a moving mass at the other end", *Proceedings of the 28th International Congress on Sound and Vibration*, Singapore, July.

Etiwa, R.M., Elabsy, H.M. and Elkaranshawy, H.A. (2021), "Finite element analysis of the longitudinal impact of a rod with various support conditions", *Int. J. Mech. Eng. Robot. Res.,* **10**(11).

Gan, C., Wei, Y. and Yang, S. (2014), "Longitudinal wave propagation in a rod with variable cross-section", *J. Sound Vib.*, **333**(2), 434-445. https://doi.org/10.1016/j.jsv.2013.09.010.

Gan, C., Wei, Y. and Yang, S. (2016), "Longitudinal wave propagation in a multi-step rod with variable cross-section", *J. Vib. Control*, **22**(3), 837-852. https://doi.org/10.1177/1077546314531806.

Goldsmith, W. (1960), *Impact: The theory and physical behavior of colliding solids*, (1st Ed.), Edward Arnold, London.

Graff, K.F. (1975), *Wave motion in elastic solids*, Ohio State Univ. Press, Columbus, USA.

Gunawan, A. and Hirose, S. (2005), "Boundary element analysis of guided waves in a bar with an arbitrary cross-section", *Eng. Anal. Bound. Elem.*, **29**(10), 913-924. https://doi.org/10.1016/j.enganabound.2005.05.007.

Guo, S. and Yang, S. (2015), "Longitudinal vibrations of arbitrary non-uniform rods", *Acta Mechanica Solida Sinica*, **28**(2), 187-199. https://doi.org/10.1016/S0894-9166(15)30007-0.

Guo, S. and Yang, S. (2012), "Wave motions in non-uniform one-dimensional waveguides", *J. Vib. Control*, **18**(1), 92-100.

https://doi.org/10.1177/1077546311399948.
Hu, B., Eberhard, P. and Schiehlen, W. (1999), "Solving wave propagation problems symbolically using computer Algebra", *Dyn. Vibro-Impact Syst.*, 231-240.
Hu, B., Eberhard, P. and Schiehlen, W. (2001), "Symbolical impact analysis for a falling conical rod against the rigid ground", *J. Sound Vib.*, **240**(1), 41-57. https://doi.org/10.1006/jsvi.2000.3200.
Hu, B. and Eberhard, P. (2004), "Simulation of longitudinal impact waves using time delayed systems", *J. Dyn. Syst. Measure. Control*, **126**, 644-649. https://doi.org/10.1115/1.1789539.
Hull, A.J. (2018), "A modal solution for finite length rods with non-uniform area", *Appl. Sci.*, **8**, 1-16. https://doi.org/10.3390/app8010094.
Idesman, A.V., Subramanian, K., Schmidt, M., Foley, J.R., Tu, Y. and Sierakowski, R.L. (2010), "Finite element simulation of wave propagation in an axisymmetric bar", *J. Sound Vib.*, **329**(14), 2851-2872. https://doi.org/10.1016/j.jsv.2010.01.021.
Jiao, X.J. and Ma, J.M. (2016), "The analysis of longitudinal impact response for variable cross-section rod", *Key Eng. Mater.*, **693**, 504-510. https://doi.org/10.4028/www.scientific.net/KEM.693.504.
Johnson, W. (1972), *Impact strength of materials,* (1st Ed.), Edward Arnold, London.
Krehl, P.O.K. (2008), *History of Shock Waves, Explosions and Impact: A Chronological and Biographical Reference,* Springer Science & Business Media.
Korzyuk, V.I. and Rudzko, J.V. (2024), "Classical solution to mixed problems from the theory of longitudinal impact on an elastic semi-infinite rod in the case of separation of the impacting body after the collision", *Proceedings of the national academy of sciences of Belarus, Physics and mathematics series* **60**(2), 95-105. https://doi.org/10.29235/1561-2430-2024-60-2-95-105.
Kumar, K.V., Saravanan, T.J., Sreekala, R., Gopalakrishnan, N. and Mini, K.M. (2017), "Structural damage detection through longitudinal wave propagation using spectral finite element method", *Geomech. Eng.*, **12**(1), 161-183.
Liu, L., Wang, Y., Qian, Y. and Li, S. (2022), "Dynamic analysis of sonic vibration drilling string with the sampling tool", *Alexandria Eng. J.*, **61**(11), 8703-8713. https://doi.org/10.1016/j.aej.2022.02.012.
Love, A.E.H. (1944), *A treatise on the mathematical theory of elasticity*, (4th Ed.), Dover Publications, New York, USA.
Malla, R.B. and Vila, L.J. (2017), "Dynamic impact force in an axial member with coupled effects of structural vibration and various support conditions", *Eng. Struct.*, **144**, 210-224. https://doi.org/10.1016/j.engstruct.2017.04.040.
Nunes, A.W., da Silva, S. and Ruiz, A. (2022), "Exact general solutions for the mode shapes of longitudinally vibrating mon-uniform rods via lie symmetries", *J. Sound Vib.*, 538. https://doi.org/10.1016/j.jsv.2022.117216.
Pala, Y., and Kahya, Ç. (2022), "A method based on Riccati equation for the vibration analysis of rods with variable cross-sections", *Int. J. Struct. Stab. Dyn.*, **22**(11). https://doi.org/10.1142/S0219455422501231.
Ragab, S.A. and Fayed, H.E. (2018), *Introduction to finite element analysis for engineers*, (1st Ed.), CRC Press, Taylor & Francis Group.
Ramírez, H. and Rubio-Gonzalez, C. (2006), "Finite-element simulation of wave propagation and dispersion in Hopkinson bar test", *Mater. Design*, **27**(1), 36-44. https://doi.org/10.1016/j.matdes.2004.08.021.
Sankin, Y.N. and Yuganova, N.A. (2001), "Longitudinal vibrations of elastic rods of stepwise-variable cross-section colliding with a rigid obstacle", *J. Appl. Math. Mech.*, **65**(3), 427-433. https://doi.org/10.1016/S0021-8928(01)00048-X.
Schwarz, C., Fischer, F.D., Werner, E. and Dirschmid, H.J. (2010), "Impact of an elastic rod on a deformable barrier : Analytical and numerical investigations on models of a valve and a rod-shaped stamping tool", *Arch. Appl. Mech.*, **80**(1), 3-24. https://doi.org/10.1007/s00419-009-0361-7.
Shen, Y. and Yin, X. (2014), "Dynamic substructure analysis of stress waves generated by impacts on non-uniform rod structures", *Mechanism and Machine Theory*, **74**, 154-172. https://doi.org/10.1016/j.mechmachtheory.2013.12.004.
Shen, Y. and Yin, X. (2016), "Analysis of geometric dispersion effect of impact-induced transient waves in composite rod using dynamic substructure method", *Appl. Math. Model.,* **40**(3), 1972-1988. https://doi.org/10.1016/j.apm.2015.09.022.
Stepanov, R., Romenskyi, D. and Tsarenko, S. (2018), "Dynamics of longitudinal impact in the variable cross-section rods", *IOP Conference Series: Mater. Sci. Eng.*, **317**(1). https://doi.org/10.1088/1757-899X/317/1/012029.
Timoshenko, S. (1937), *Vibration problems in engineering*, (2nd Ed.), D. Van Nostrand Company Inc., New York, USA.
Ulitin, G.M. and Tsarenko, S.N. (2018), "Dynamics of longitudinal impact of an inhomogeneous rod on a limit", *J. Theor. Appl. Mech.*, **64-65**(3-4), 43-50.
Ulitin, G.M. and Tsarenko, S.N. (2015), "Longitudinal vibrations of elastic rods of variable cross-section", *Int. Appl. Mech.*, **51**(1), 102-107. https://doi.org/10.1007/s10778-015-0676-8.
Ulitin, G.M. and Tsarenko, S.N. (2016), "Method of averaging for the tasks on longitudinal impact of variable section rods", *Math. Mech. Phys.,* **8**(1), 43-48.
Utyashev, I. (2019), "Longitudinal oscillation of a rod with a variable cross section", *Multiphase Syst.*, **14**(2), 138-141. https://doi.org/10.21662/mfs2019.2.019.
Vila, L.J., and Malla, R.B. (2014), "Longitudinal impact force on a special drill for planetary exploration", *Earth and Space*, 404-413.
Wang, A. and Tian, W. (2007), "Mechanism of buckling development in elastic bars subjected to axial impact", *Int. J. Impact Eng.*, **34**(2), 232-252. https://doi.org/10.1016/j.ijimpeng.2005.07.005.
Wang, Y., Wang, T. and Ye, X. (2024), "Semi-analytical solution to elastic–plastic contact-impact between a 316 stainless steel rod with truncated cone nose and rigid flat", *Int. J. Solid. Struct.,* **291**, 112702. https://doi.org/10.1016/j.ijsolstr.2024.112702.
Wang, T., Wang, Y., Ye, X. and Huang, G. (2023), "Elastoplastic impact of a long rod on a flexible large plate", *Int. J. Impact Eng.*, **177**, 104586. https://doi.org/10.1016/j.ijimpeng.2023.104586.
Xu, D., Du, J. and Liu, Z. (2019), "An accurate and efficient series solution for the longitudinal vibration of elastically restrained rods with arbitrarily variable cross sections", *J. Low Freq. Noise V. A.*, **38**(2), 403-414. https://doi.org/10.1177/1461348419825913.
Yang, K. (2008), "A unified solution for longitudinal wave propagation in an elastic rod", *J. Sound Vib.*, **314**(1-2), 307-329. https://doi.org/10.1016/j.jsv.2008.01.007.
YuFeng, X. and DeChao, Z. (1998), "Analytical solutions of impact problems of rod structures with springs", *Comput. Method. Appl M.*, **160**(3-4), 315-323. https://doi.org/10.1016/S0045-7825(97)00296-X.

CC